Magnetic structures and (x,T) magnetic phase diagram of $ZrMn_6Sn_{6-x}Ga_x$

2005 J. Phys.: Condens. Matter 17 1547

(http://iopscience.iop.org/0953-8984/17/10/010)

INSTITUTE OF PHYSICS PUBLISHING JOURNAL OF PHYSICS: CONDENSED MATTER

J. Phys.: Condens. Matter **17** (2005) 1547–1560 doi:10.1088/0953-8984/17/10/010

Magnetic structures and (x, T) magnetic phase diagram of $ZrMn_6Sn_{6-x}Ga_x$

Thomas Mazet[1,4], **Olivier Isnard**[2,3] **and Bernard Malaman**[1]

[1] Laboratoire de Chimie du Solide Minéral, Université Henri Poincaré-Nancy I, Associé au CNRS (UMR 7555), BP 239, 54506 Vandoeuvre lès Nancy Cedex, France
[2] Laboratoire de Cristallographie (CNRS) associé à l'Université J Fourier, BP 166, 38042 Grenoble Cedex 9, France
[3] Institut Universitaire de France, Maison des Universités, 103 boulevard Saint Michel, 75005 Paris, France

E-mail: thomas.mazet@lcsm.uhp-nancy.fr

Received 14 December 2004, in final form 27 January 2005
Published 25 February 2005
Online at stacks.iop.org/JPhysCM/17/1547

Abstract

$ZrMn_6Sn_{6-x}Ga_x$ ($0.25 \leqslant x \leqslant 3.50$) compounds of $HfFe_6Ge_6$-type structure ($P6/mmm$) have been studied using powder neutron diffraction experiments in the 2–600 K temperature range. Below their magnetic ordering temperatures, these phases adopt commensurate easy-plane magnetic arrangements: $+--+$ antiferromagnetic AF2 ($x \leqslant 0.60$) or ferromagnetic ($x \geqslant 0.70$). At low temperature, the Ga-poor compounds ($x \leqslant 0.80$) exhibit a transition to concentration-dependent incommensurate configurations. Upon increasing the Ga content, this incommensurate state evolves from helimagnetic to *fan-like* through arrangements we termed *antifan-like*. The Mn moment value is close to $m_{Mn} \approx 2.0\ \mu_B$ for the Ga-rich and Ga-poor compounds and reaches a maximum amplitude of $m_{Mn} \approx 3.0\ \mu_B$ in the *(anti)fan-like* structures of intermediate concentrations. A tentative (x, T) magnetic phase diagram is presented. The occurrence of Lifshitz point(s) is forecast for $0.60 < x < 0.70$.

1. Introduction

The magnetic properties of the Mn sublattice of ternary RMn_6Sn_6 and pseudo-ternary $RMn_6Sn_{6-x}X'_x$ ($X' =$ Ga or In) involving a non-magnetic R element can be tuned by modifying the R and/or average p element valences [1–7, 13]. It was first found that the magnetic behaviour of RMn_6Sn_6 evolves with the valence of R. To summarize (see section 2 for details), divalent R compounds (R = Mg, Ca or Yb) are ferromagnets ($T_C \approx 290$ K) [2, 4] and trivalent R compounds (R = Sc, Y or Lu) are helimagnets ($T_N \approx 350$ K) [1] while tetravalent R compounds (R = Zr or Hf) are antiferromagnets ($T_N \approx 570$ K) [3]. The lack of

[4] Author to whom any correspondence should be addressed.

$R_{1-x}R'_xMn_6Sn_6$ solid solutions (R = a divalent atom, R′ = a trivalent or tetravalent atom) [3] has prevented observation of the crossover from ferromagnetism to antiferro(heli)magnetism of the Mn sublattice. This was achieved later by partially substituting Ga or In for Sn in compounds involving trivalent R atoms [5–7]. Decreasing the average valence of the p element has globally the same effect as decreasing the valence of R. This yields a decrease of the ordering temperature and the stabilization of a ferromagnetic order for sufficiently high Ga or In contents. The intermediate compositions undergo ferromagnetic to helimagnetic transition upon cooling [11, 12] and exhibit a low-field metamagnetic behaviour [5–7]. Giant magnetoresistance (GMR) phenomena are often observed at the metamagnetic transition [5, 8–10]. Hence, in addition to their potential technological interest due to their GMR properties, $RMn_6Sn_{6-x}X'_x$ (X′ = In or Ga) solid solutions are excellent systems for studying competing ferro- and antiferromagnetic exchange interactions.

Synthesis of $ZrMn_6Sn_{6-x}Ga_x$ ($x \leqslant 3.75$) has allowed us to study, for the first time, the magnetic properties of solid solutions involving tetravalent R [13]. The Ga substitution yields for sufficiently high Ga contents ($x \geqslant 0.90$) the stabilization of a ferromagnetic order, as is the case for trivalent R, but with higher Curie temperatures. The Ga-poor ($x \leqslant 0.60$) compounds preserve antiferromagnetic properties, their low temperature macroscopic magnetic behaviour being overshadowed by the presence of the *ferromagnetic-like* Mn_3Sn_2 impurity ($T_C \approx 270$ K). Compounds with intermediate Ga contents ($0.60 < x \leqslant 0.80$) order ferromagnetically ($T_C \approx 465$ K) and present a marked decrease in their magnetization at lower temperature. Unlike the trivalent R compounds, the magnetization curves at 5 K do not exhibit any abrupt upward curvature but a *ferromagnetic-like* behaviour characterized by a weaker initial susceptibility than that of the pure ferromagnets ($x \geqslant 0.90$). This difference in the field dependence between trivalent R compounds and tetravalent R compounds probably originates from different zero-field magnetic configurations.

In this paper, we investigate the zero-field magnetic structures of $ZrMn_6Sn_{6-x}Ga_x$ ($0.25 \leqslant x \leqslant 3.50$) using powder neutron diffraction experiments. The organization of the paper is as follows. The crystal and magnetic structures previously found in RMn_6Sn_6 and $RMn_6Sn_{6-x}X'_x$ (X′ = In or Ga) are described in section 2. Section 3 deals with experimental details. The results are presented and discussed in section 4. Finally, a conclusion is given in section 5.

2. Crystal and magnetic structures

RMn_6Sn_6 and $RMn_6Sn_{6-x}X'_x$ (X′ = In or Ga) crystallize in the pseudo-lamellar $HfFe_6Ge_6$-type structure ($P6/mmm$) or its partially disordered derivatives. The $HfFe_6Ge_6$-type (figure 1) comprises one R site, one Mn site and three sites (2c, 2d and 2e) for the p elements (X = Sn; X′ = Ga or In). RMn_6Sn_6 of $HfFe_6Ge_6$ type can be described as an alternative stacking of two different slabs along the c-axis: the Mn–Sn(2e)–Sn(2c)–Sn(2e)–Mn slab (the X-slab) and the Mn–[R, Sn(2d)]–Mn slab (the R-slab). It has been found that in pseudo-ternary $RMn_6Sn_{6-x}X'_x$ (X′ = In or Ga) the Ga atoms preferentially occupy the 2d site of lowest Wigner–Seitz cell volume whereas the larger In atoms mainly substitute for Sn in the 2c site [11–13].

Three kinds of magnetic structure have been found in RMn_6Sn_6 with non-magnetic R (figure 1): ferromagnetic, helimagnetic and $+--+$ antiferromagnetic (AF2) [1, 3, 4]. These magnetic arrangements are built upon ferromagnetic easy-plane (001) Mn sheets. The interlayer Mn–Mn coupling is always ferromagnetic (or nearly) through the X-slab. Conversely, the Mn–Mn coupling through the R-slab strongly depends on temperature and R. This coupling is collinear in the ferromagnetic ($\boldsymbol{k} = \langle 0, 0, 0\rangle$) RMn_6Sn_6 with divalent R (= Yb, Mg, Ca) [4]. It is antiferromagnetic above the commensurate–incommensurate

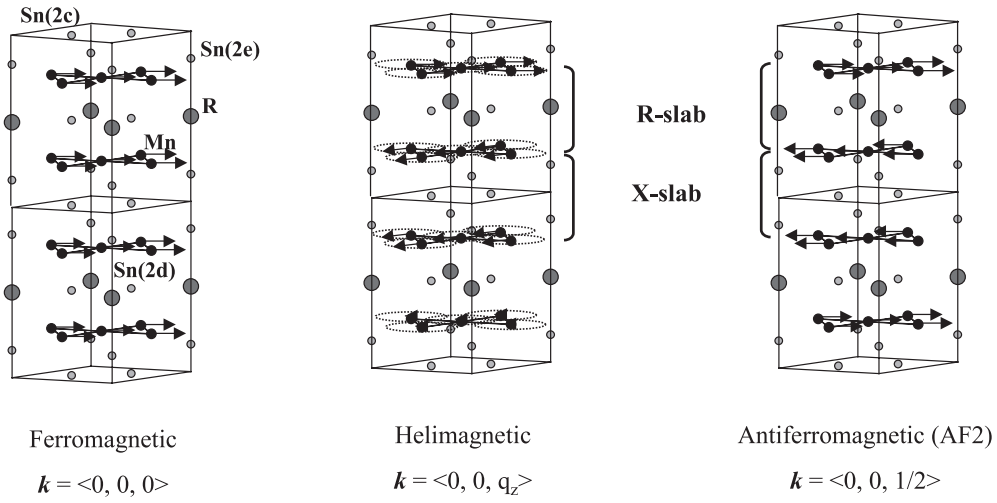

Figure 1. Crystal and magnetic structures of RMn_6Sn_6 and $RMn_6Sn_{6-x}X'_x$ (X′ = Ga or In). In the $HfFe_6Ge_6$-type structure, R atoms occupy the 1b site (0, 0, $\frac{1}{2}$), the Mn atoms occupy the 6i site ($\frac{1}{2}$, 0, $z_{Mn} \approx 0.25$) and the Sn atoms occupy the 2c, 2d and 2e sites in ($\frac{1}{3}$, $\frac{2}{3}$, 0), ($\frac{1}{3}$, $\frac{2}{3}$, $\frac{1}{2}$) and (0, 0, $z_{Sn(2e)} \approx 0.17$), respectively.

transition temperature $T_{CI} \approx 60$ K for tetravalent R (= Zr, Hf) leading to the $+ - -+$ antiferromagnetic (AF2) structure ($\boldsymbol{k} = \langle 0, 0, 1/2 \rangle$). Below this transition temperature, $ZrMn_6Sn_6$ and $HfMn_6Sn_6$ present helimagnetic arrangements ($\boldsymbol{k} = \langle 0, 0, q_z \rangle$) with a weakly temperature dependent q_z component. At 2 K, $q_z \approx 0.485$ rlu (reciprocal lattice units) and the Mn–Mn coupling through the R-slab deviates by approximately 10° from perfect antiferromagnetic alignment [3]. Within trivalent R compounds (R = Sc, Y, Lu), except $LuMn_6Sn_6$ above 200 K which also exhibits the AF2 structure, the coupling is non-collinear, yielding helimagnetic configurations characterized by weaker q_z values ($0.20 < q_z < 0.40$ rlu) which decrease with temperature [1]. At 2 K, the angle between Mn moments of adjacent planes is close to 90° within the R-slab. Unlike the ordering temperatures which strongly decrease from $T_N \approx 570$ K (R = Zr, Hf) [3] down to $T_C \approx 250$ K in $Mg_{1-x}Ca_xMn_6Sn_6$ [2], the Mn moment magnitude remains nearly constant throughout the RMn_6Sn_6 series and close to 2.2 μ_B at 2 K.

$RMn_6Sn_{6-x}X'_x$ (X′ = In or Ga) solid solutions involving non-magnetic trivalent R have been less intensively studied by neutron diffraction [11, 12]. Despite the fact that In and Ga substitutions preferentially take place in two different slabs and yield opposite variation of the cell parameters, they modify in the same way the magnetic behaviour of the Mn sublattice. The low substituted phases behave like the ternary parent compounds while the more substituted ones are ferromagnetic. The intermediate compositions exhibit ferromagnetic to helimagnetic transition upon cooling. The helimagnetic configurations are characterized by q_z values in the 0.10–0.40 rlu range depending on temperature and X′ concentration. The In/Ga substitution may alter the Mn moment magnitude and values as large as $m_{Mn} = 2.7$ μ_B have been reported in $RMn_6Sn_{6-x}X'_x$ [12]. Note that, in all cases, no change of the Mn moment value is observed at the commensurate–incommensurate transition.

It is quite clear that the magnetic behaviour of these systems is mainly driven by valence electron concentration (VEC) while Mn–Mn interatomic distances only play a secondary role. Mn–Mn interplanar RKKY-type exchange interactions are undoubtedly involved

and incommensurate orders are stabilized because of antagonistic antiferromagnetic and ferromagnetic interactions. The chemical nature of the R element is also an influent parameter, probably through hybridization of its valence states with the 3d Mn states [14], since trivalent R and tetravalent R compounds exhibit certain differences in their magnetic properties, especially as regards their field dependence and ordering temperatures [13].

3. Experimental details and refinement procedure

The investigated $ZrMn_6Sn_{6-x}Ga_x$ powder samples were those we used in [13]. An annealing treatment (3 weeks at 650 °C) has been performed in order to homogenize the samples, leading to a single phase of 166 according to our previous x-ray and microprobe investigations. Only small amounts (i.e. a few wt%) of β-Sn, Mn_3Sn_2, $MnSn_2$ or $ZrGa_2$ have been found as impurity [13]. Powder neutron diffraction experiments were carried out at the Institut Laue Langevin, Grenoble (France) using the D1b two-axis diffractometer ($\lambda = 2.52$ Å, step of 0.2°). Due to the limited beam time, only some selected compositions were studied ($x = 0.25$, 0.50, 0.60, 0.80, 1.00, 2.00 and 3.50). The patterns were recorded in the 2–300 K temperature range using a standard cryostat while the compounds with $x = 0.50$, 0.60 and 0.80 were also studied between 300 and 600 K in a furnace.

The analysis of the patterns was performed by Rietveld profile refinements using the software Fullprof [15]. The nuclear contribution arising from the impurities previously detected by x-ray diffraction was taken into account during the refinement procedure. To avoid a too large number of intensity dependent parameters we kept the Ga occupancy ratio fixed to the values found from our previous refinements of x-ray data [13]. The shape of the diffraction peaks was fitted using a pseudo-Voigt function. Besides the peak profile parameters, the fits comprised scale factor, zero shift, cell parameters, crystallographic-position parameters (z_{Mn} and $z_{Sn/Ga(2e)}$) and magnetic parameters (see below for details). The overall temperature factor (B_{ov}) was fixed to reasonable values, e.g. 1.5, 1.0 and 0.1 Å^2 at $T = 600$, 300 and 2 K, respectively. The R_{wp} and R_e Rietveld agreement factors given here correspond, respectively, to the expected and weight profile factors as defined in [16] while R_n and R_m are the Bragg agreement factors calculated for, respectively, the nuclear and magnetic contribution to the diffraction pattern.

4. Results and discussion

4.1. The low substituted compound ($x = 0.25$)

The compound with $x = 0.25$ behaves similarly to $ZrMn_6Sn_6$ [3]. Between 300 K and $T_{CI} = 75 \pm 5$ K, the $\boldsymbol{k} = \langle 0, 0, 1/2\rangle$ magnetic satellites (figure 2) characteristic of the AF2 magnetic structure are observed. Below T_{CI}, these magnetic peaks undergo splitting. The new Bragg peaks can be indexed using a wavevector $\boldsymbol{k} = \langle 0, 0, q_z\rangle$, whose q_z component slightly decreases upon cooling (inset of figure 2) down to $q_z = 0.475(1)$ rlu at 2 K. In the corresponding in-plane helical arrangement, the orientation of the Mn moment $\boldsymbol{m}_{Mn}$ is given by

$$\boldsymbol{m}_{Mn} = m_{Mn}\cos(\boldsymbol{k}\cdot\boldsymbol{R}_n + \varphi)\boldsymbol{u} + m_{Mn}\sin(\boldsymbol{k}\cdot\boldsymbol{R}_n + \varphi)\boldsymbol{v}. \quad (1)$$

Here, $\boldsymbol{u}$ and $\boldsymbol{v}$ are orthogonal unit vectors in the basal plane, $\boldsymbol{R}_n$ is the position vector in the nth chemical cell and φ is the phase angle. The phase origin was chosen at the Mn layer in $z \approx \frac{1}{4}$. The refined parameters and the residual factor values are given in table 1. Similarly to what has been found for $ZrMn_6Sn_6$ [3], the angle between Mn moments of two adjacent

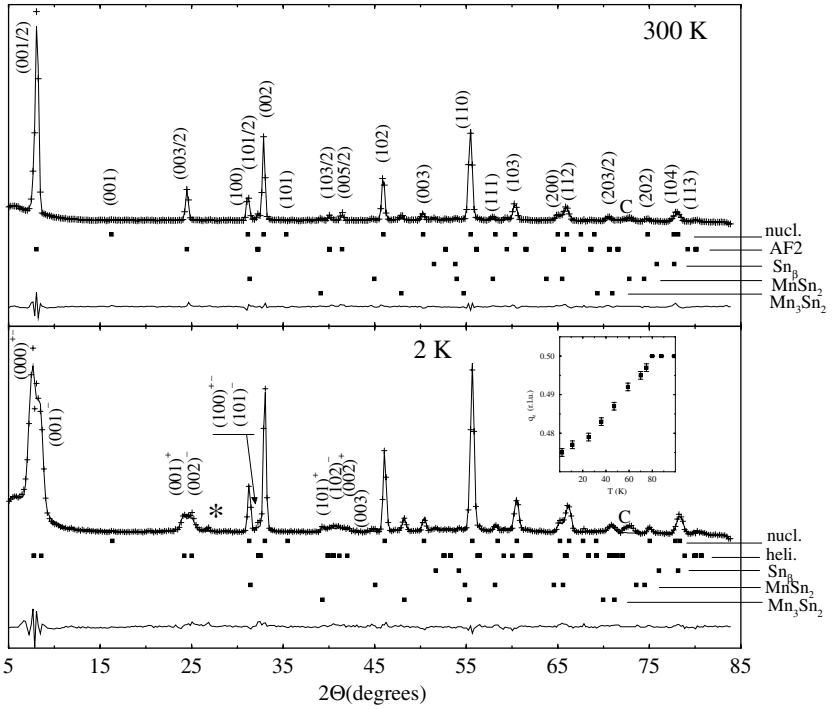

Figure 2. Neutron diffraction patterns of $ZrMn_6Sn_{5.75}Ga_{0.25}$ at 300 and 2 K. The star indicates a magnetic peak of the Mn_3Sn_2 impurity. C marks peaks arising from the tail of the cryostat. The inset shows the thermal evolution of the q_z component of the wavevector below 100 K.

Table 1. Refined parameters of $ZrMn_6Sn_{6-x}Ga_x$ ($x = 0.25$, 1.00, 2.00, 3.50) from neutron diffraction data at 300 and 2 K.

x	0.25		1.00		2.00		3.50	
T (K)	300	2	300	2	300	2	300	2
a (Å)	5.441(1)	5.426(1)	5.391(1)	5.369(1)	5.351(1)	5.331(1)	5.292(1)	5.273(1)
c (Å)	8.939(2)	8.908(3)	8.854(3)	8.819(3)	8.762(2)	8.728(2)	8.668(3)	8.631(3)
z_{Mn}	0.258(1)	0.257(2)	0.257(1)	0.255(2)	0.261(1)	0.260(1)	0.257(2)	0.256(2)
$z_{Sn/Ga(2e)}$	0.176(2)	0.176(2)	0.177(1)	0.179(2)	0.175(1)	0.176(2)	0.169(2)	0.168(2)
m_{Mn} (μ_B)	1.88(2)	2.08(2)	1.97(5)	2.43(5)	1.83(5)	2.34(5)	0.59(18)	2.00(8)
q_z (rlu)	1/2	0.475(1)	0	0	0	0	0	0
φ (deg)	—	91(1)	—	—	—	—	—	—
R_n, R_m (%)	4.92, 6.04	5.20, 7.99	4.01, 9.57	6.22, 6.89	3.54, 6.45	2.62, 5.33	4.01, 13.2	3.25, 7.84
R_{wp}, R_e (%)	11.0, 2.45	11.4, 3.10	11.0, 3.88	10.3, 3.31	9.09, 3.99	9.27, 4.16	13.3, 5.37	12.7, 5.16

planes is $\approx 170°$ through the R-slab and about $\approx 0°$ through the X-slab. No change of the Mn moment magnitude is observed at the commensurate–incommensurate transition.

4.2. The ferromagnetic Ga-rich phases ($x = 1.00$, 2.00 and 3.50)

As expected from magnetic measurements, the compounds richer in Ga behave as simple ferromagnets. At 300 and 2 K the diffraction peaks can all be indexed using the chemical cell (figure 3) while the strong increase of the (002) line indicates that the Mn moments lie in

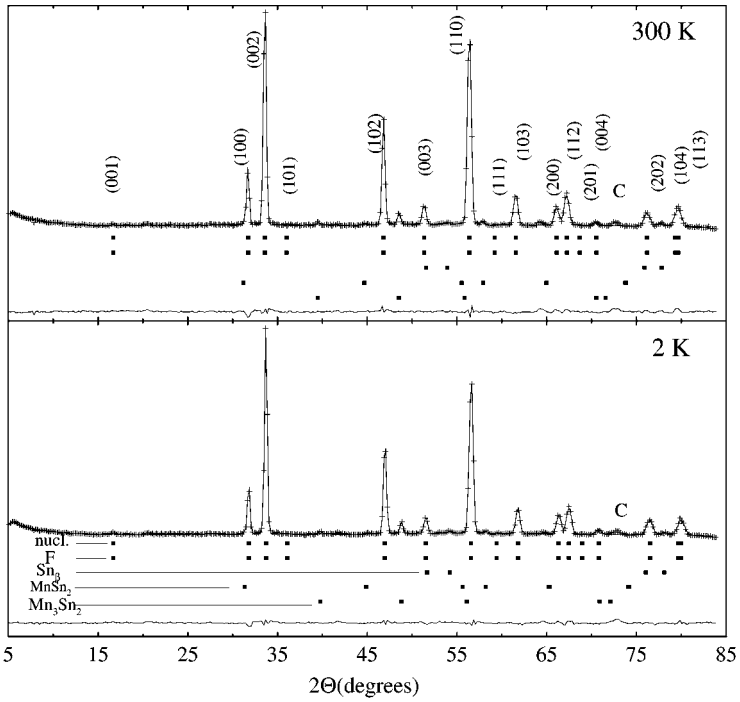

Figure 3. Neutron diffraction patterns of $ZrMn_6Sn_{4.00}Ga_{2.00}$ at 300 and 2 K. C marks peaks arising from the tail of the cryostat.

or close to the basal plane. The better refinements lead to place the Mn moment in the basal plane. Thus, similarly to all others $RMn_6Sn_{6-x}X'_x$ (X′ = In or Ga) with sufficiently high X′ contents, the ferromagnetic arrangement of these compounds is identical to that of RMn_6Sn_6 with divalent R: ferromagnetic easy-plane (001) Mn sheets coupled ferromagnetically (see figure 1). At 2 K, the refined Mn moment value (table 1) is found to slightly decrease upon increasing the Ga content from $m_{Mn} = 2.43(5)\ \mu_B$ for $x = 1.00$ down to $m_{Mn} = 2.00(8)\ \mu_B$ for $x = 3.50$, in reasonable agreement with magnetization measurements. As for the rest of the series, the low R_n (3–5%) values corroborate the Ga atom distribution found from previous x-ray refinements [13].

4.3. $x = 0.50, 0.60$ and 0.80: the fan-like structures

4.3.1. Thermal behaviour of the neutron patterns. Neutron diffraction patterns were recorded in the 2–600 K temperature range (figures 4 and 5). They indicate that below their magnetic ordering point these compounds adopt commensurate magnetic arrangements (figure 1): either the AF2 arrangement ($\boldsymbol{k} = \langle 0, 0, 1/2\rangle$) for $x = 0.50$ and $x = 0.60$ ($T_N = 495 \pm 5$ K and $T_N = 465 \pm 5$ K, respectively) or the simple easy-plane ferromagnetic arrangement ($\boldsymbol{k} = \langle 0, 0, 0\rangle$) for $x = 0.80$ ($T_C = 475 \pm 10$ K). These ordering temperatures are close to those found from magnetic measurements [13]. The refined parameters in the paramagnetic state and at 300 K are given in table 2. The thermal variation of the cell parameters exhibits no anomaly between 2 and 600 K (figure 6).

Below a concentration-dependent transition temperature T_{CI} ($= 95 \pm 5$ K, 270 ± 5 K and 150 ± 5 K for $x = 0.50$, 0.60 and 0.80, respectively), the neutron diffraction patterns

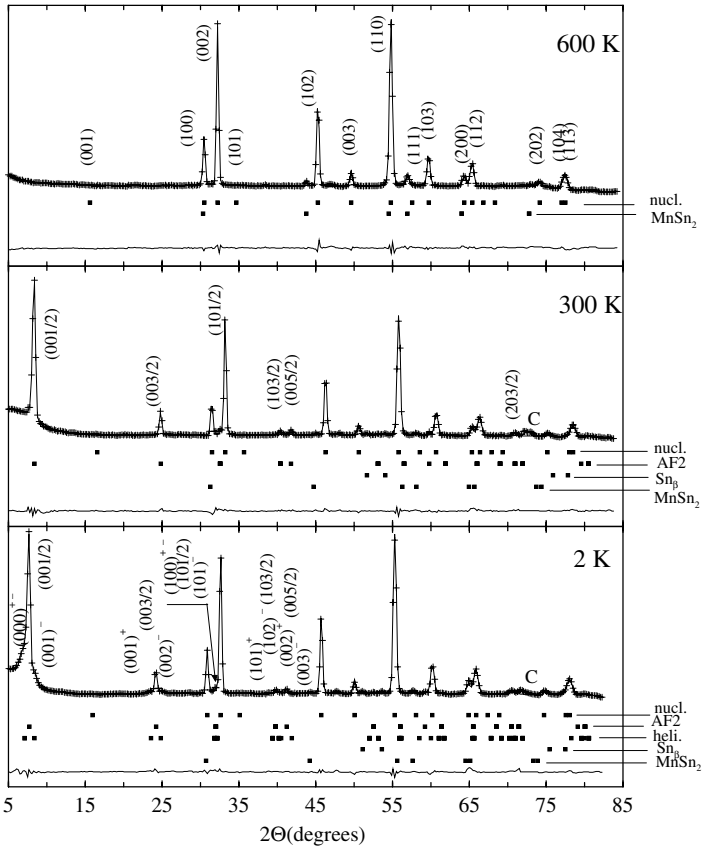

Figure 4. Neutron diffraction patterns of $ZrMn_6Sn_{5.40}Ga_{0.60}$ at 600, 300 and 2 K. C marks peaks arising from the tail of the cryostat.

Table 2. Refined parameters of $ZrMn_6Sn_{6-x}Ga_x$ ($x = 0.50, 0.60, 0.80$) from neutron diffraction data in the paramagnetic state and at 300 K.

x	0.50		0.60		0.80	
T (K)	600	300	600	300	540	300
a (Å)	5.464(1)	5.425(1)	5.460(1)	5.418(1)	5.436(1)	5.404(1)
c (Å)	8.978(1)	8.922(3)	8.959(3)	8.904(2)	8.924(2)	8.875(2)
z_{Mn}	0.257(1)	0.259(1)	0.258(2)	0.258(1)	0.260(1)	0.258(1)
$z_{Sn/Ga(2e)}$	0.177(1)	0.174(2)	0.176(2)	0.173(1)	0.176(1)	0.175(1)
m_{Mn} (μ_B)	—	1.80(2)	—	1.45(1)	—	1.93(4)
q_z (rlu)	—	1/2	—	1/2	—	0
R_n, R_m (%)	3.31, —	3.96, 9.09	5.75, —	5.55, 7.79	5.64, —	4.11, 6.82
R_{wp}, R_e (%)	8.92, 2.31	12.9, 3.95	13.4, 7.05	8.71, 2.38	10.4, 2.17	7.01, 3.14

evolve in a somewhat similar manner. The intensity of the main magnetic peaks ((001/2) and (003/2) for $x = 0.50$ and 0.60; (002) and (102) for $x = 0.80$) decreases upon cooling while new magnetic satellites growth on both sides of these commensurate peaks. In each case, the new satellites can be indexed using an incommensurate wavevector $\boldsymbol{k}' = \langle 0, 0, q_z \rangle$. Only first-order satellites were detected, no second-order satellite. For $x = 0.50$ and 0.60, the q_z

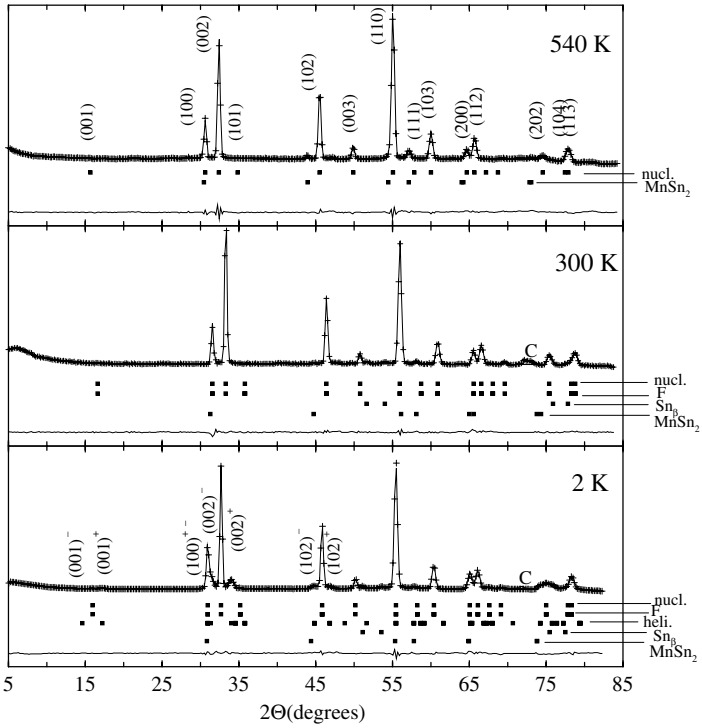

Figure 5. Neutron diffraction patterns of $ZrMn_6Sn_{5.20}Ga_{0.80}$ at 540, 300 and 2 K. C marks peaks arising from the tail of the cryostat.

component is, within the error bar, independent of temperature and close to $q_z = 0.465$ rlu. For $x = 0.80$, q_z slightly increases upon cooling up to $q_z = 0.078(2)$ rlu at 2 K (see the inset of figure 6). The intensity of both the commensurate and incommensurate magnetic peaks evolves over a limited temperature range, before remaining almost constant down to 2 K (figure 7). Hence, the commensurate and incommensurate components are simultaneously present over the entire temperature range below T_{CI}. The occurrence of strong $(00l)^{\pm}$ reflections implies that the moments of the incommensurate components are in (or close to) the basal plane. The $\boldsymbol{k}' = \langle 0, 0, q_z \rangle$ satellites can indeed be fitted assuming an incommensurate arrangement (helical or sine-wave modulated) built upon ferromagnetic easy-plane (001) Mn sheets.

4.3.2. Possible models. When two sets of magnetic satellites coexist, powder neutron diffraction cannot distinguish if they arise from two distinct magnetic phases or come from a unique magnetic phase [17]. For several reasons, we were led to consider only the situation of a single magnetic phase and to rule out the possibility of an inhomogeneous mixture of two magnetic phases, linked or not to inhomogeneity in Ga concentration. First, we note that for $x = 0.50$ and 0.60, $\boldsymbol{k} = \langle 0, 0, 1/2 \rangle$ satellites are observed down to 2 K while the corresponding $+--+$ AF2 arrangement is not stable at this temperature for compounds with lower Ga contents (see section 4.1). Secondly, the fact that the two sets of satellites coexist over a large temperature range while their intensity changes concomitantly over a limited temperature range (figure 7) also speaks in favour of a single phase. The small variations of the Ga content within the sample are more likely to be responsible for a certain spread in transition temperature.

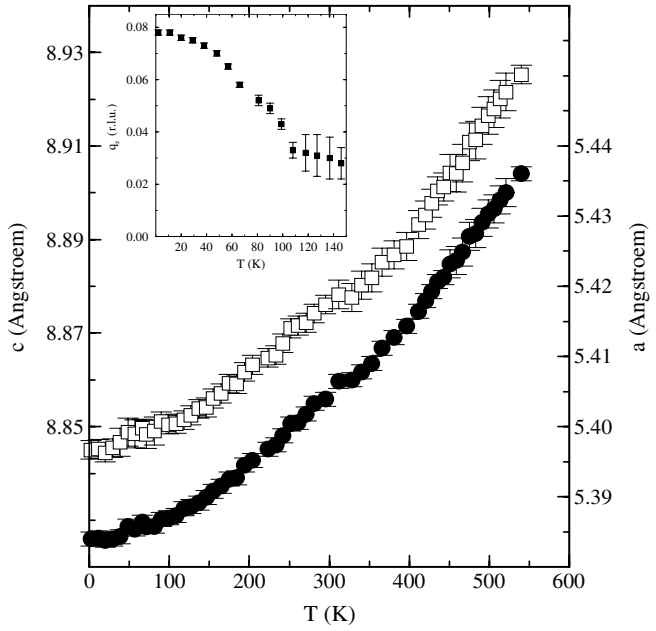

Figure 6. Temperature dependence of the cell parameters of $ZrMn_6Sn_{5.20}Ga_{0.80}$ between 540 and 2 K (c-parameter, □, left scale; a-parameter, ●, right scale). The inset shows the thermal evolution of the q_z component of the wavevector below 150 K.

As previously discussed by Schobinger-Papamentellos *et al* [18, 19], once it is assumed that the two wavevectors belong to a single magnetic phase, several models may be considered. For the sake of clarity, we first restrict the discussion to the $x = 0.80$ case ($\boldsymbol{k} = \langle 0, 0, 0\rangle$ and $\boldsymbol{k}' = \langle 0, 0, q_z \approx 0.08\rangle$) before extending our conclusions to $x = 0.50$ and 0.60 ($\boldsymbol{k} = \langle 0, 0, 1/2\rangle$ and $\boldsymbol{k}' = \langle 0, 0, q_z \approx 0.46\rangle$). The absence of second order satellites seems to indicate that the low temperature magnetic structure of $ZrMn_6Sn_{5.2}Ga_{0.8}$ is not a pure fan structure (FAN). However, if present, these satellites should be very weak [22] and most likely indiscernible from the background. Hence, the occurrence of a pure fan structure in $ZrMn_6Sn_{5.2}Ga_{0.8}$ at low temperature cannot be definitely ruled out. Such structure is generally observed when a magnetic field is applied in the plane of a helimagnet [20–22] but has sometimes been met in zero applied field [23]. Since only first order satellites are detected, they may arise from a sine-wave-modulated component ($\boldsymbol{m}_{\text{sine}}$) transverse to the in-plane ferromagnetic component ($\boldsymbol{m}_{\text{F}}$):

$$\boldsymbol{m}_{\text{sine}} = m_{\text{A}} \cos(\boldsymbol{k} \cdot \boldsymbol{R}_n + \varphi)\boldsymbol{u} \tag{2}$$

where m_{A} is the amplitude of the wave, $\boldsymbol{u}$ is a unit vector perpendicular to $\boldsymbol{m}_{\text{F}}$ and φ is the phase. Then the coherent superposition of $\boldsymbol{m}_{\text{sine}}$ and $\boldsymbol{m}_{\text{F}}$ (model I) corresponds to a fan-like arrangement but with a plane envelope (FAN-P). The maximal value of the Mn moment is given by $m_{\max} = \sqrt{(m_{\text{A}}^2 + m_{\text{F}}^2)}$ and the fan angle is defined as $\alpha = 2\tan^{-1}(m_{\text{A}}/m_{\text{F}})$. The second possibility (model II) is to consider that the incommensurate peaks come from an in-plane helical component $\boldsymbol{m}_{\text{heli}}$ as given by (1). Then, $m_{\text{heli}} > m_{\text{F}}$ corresponds to a distorted elliptical spiral (DS). The opposite case ($m_{\text{heli}} < m_{\text{F}}$) yields a fan-like structure with an elliptical envelope (FAN-E). In both cases the moment values range from $|m_{\text{F}} - m_{\text{heli}}|$ to $|m_{\text{F}} + m_{\text{heli}}|$. All the above described magnetic arrangements, except the pure fan structure, imply a modulation

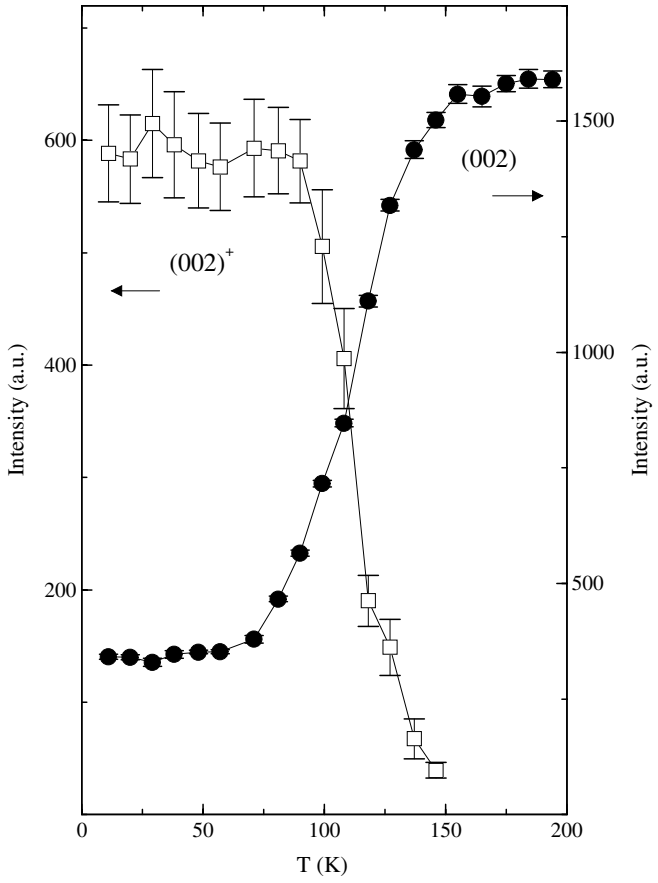

Figure 7. Thermal variation of the intensity of the commensurate (002) and incommensurate $(002)^+$ magnetic peaks in $ZrMn_6Sn_{5.20}Ga_{0.80}$ below 200 K.

of the Mn moment magnitude from plane to plane. A schematic representation of these arrangements is drawn in figure 8. We gather all these possible magnetic structures under the generic name of *fan-like* structures. By analogy, we term *antifan-like* structures all the possible arrangements resulting from the superposition of the $\boldsymbol{k} = \langle 0, 0, 1/2\rangle$ and $\boldsymbol{k}' = \langle 0, 0, q_z\rangle$ components, as is the case for $x = 0.50$ and 0.60. In the *antifan-like* structures, the semi-plane of preferred orientation of the Mn moments reverses through the R-slab. Similar antiferromagnetic fan-like structures have been reported for CeH_2/Fe multilayers [24].

4.3.3. Refinements. Below T_{CI}, the refinements were then carried out assuming a single magnetic phase consisting in the coherent superposition of two in-plane components: a commensurate one (F or AF2) and an incommensurate one (helical or sine wave) built upon ferromagnetic (001) Mn layers. It is worth noting that the $\boldsymbol{k}' = \langle 0, 0, q_z\rangle$ peaks are significantly broader than the nuclear or commensurate magnetic peaks of the same angular region. Therefore, the incommensurate satellites were fitted using a different set of profile parameters yielding better agreement factors. The broadening of the $\boldsymbol{k}' = \langle 0, 0, q_z\rangle$ peaks indicates that the degree of long-range order of the modulated component is less than that of the commensurate one. The main refined parameters at 2 K as well as the relevant *R*-values

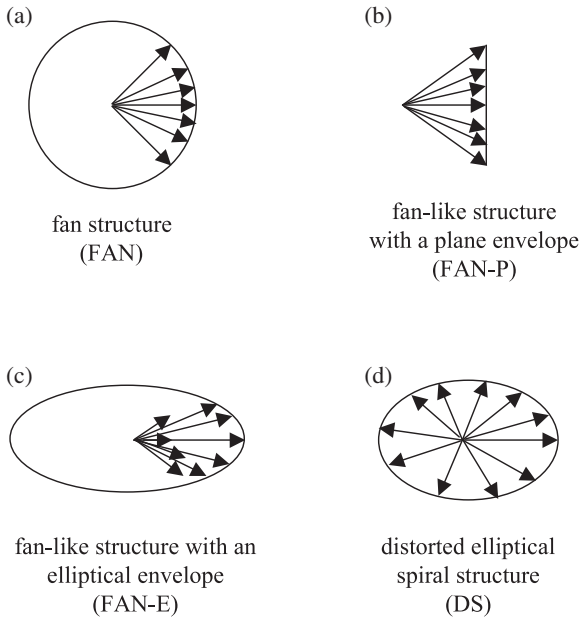

Figure 8. Schematic representation of (a) the pure fan structure (FAN); (b) the fan-like structure with a plane envelope (FAN-P); (c) the fan-like structure with an elliptical envelope (FAN-E); (d) the distorted elliptical structure (DS).

Table 3. Refined parameters of $ZrMn_6Sn_{6-x}Ga_x$ ($x = 0.50, 0.60, 0.80$) from neutron diffraction data at 2 K.

x	0.50	0.60	0.80
a (Å)	5.403(1)	5.397(1)	5.384(1)
c (Å)	8.881(1)	8.865(2)	8.845(2)
z_{Mn}	0.260(1)	0.259(1)	0.257(2)
$z_{Sn/Ga(2e)}$	0.173(1)	0.173(1)	0.178(1)
$m_{F/AF}$ (μ_B)	1.62(3)	1.25(2)	1.06(6)
m_{heli} (μ_B)	1.31(4)	0.77(5)	2.04(5)
q_z (rlu)	0.466(2)	0.463(3)	0.078(1)
φ (deg)	76(2)	73(5)	10(3)
R_n, R_m, R_{heli} (%)	2.63, 4.68, 6.49	5.54, 7.78, 10.3	3.74, 11.1, 12,6
R_{wp}, R_e (%)	8.19, 2.76	9.23, 1.08	7.61, 1.01

are given in table 3. As regards the incommensurate component, only the Mn magnetic moment value for the helical case (m_{heli}) is given. To obtain m_A (the amplitude of the sine-wave modulation) m_{heli} has to be multiplied by $\sqrt{2}$. The main magnetic parameters calculated using model I and model II are gathered in table 4. In model I, the fan angle is close to $\alpha \approx 90°$ at 2 K for $x = 0.50$ and 0.60 (ANTIFAN-P) and reaches $\alpha \approx 140°$ for $ZrMn_6Sn_{5.2}Ga_{0.8}$ (FAN-P). Model II yields a distorted spiral structure (DS) for $x = 0.80$ ($m_{heli} > m_F$) and elliptical antifan-like structures (ANTIFAN-E) for $ZrMn_6Sn_{5.5}Ga_{0.5}$ and $ZrMn_6Sn_{5.4}Ga_{0.6}$ ($m_{heli} < m_{AF}$). In all cases, the moment value is strongly enhanced at the commensurate–*(anti)fan-like* transition (figure 9) as often observed [21, 25]. Since both models lead to Mn moments of close magnitude, it is not possible to draw any conclusions based on moment values. Although the exact nature of the *(anti)fan-like* structures of the intermediate

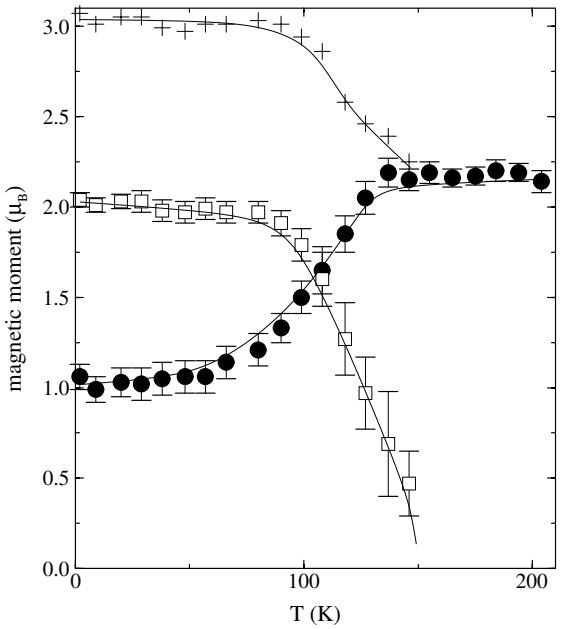

Figure 9. Temperature variation of the incommensurate $\boldsymbol{k} = \langle 0, 0, q_z \rangle$ (□) and commensurate $\boldsymbol{k} = \langle 0, 0, 0 \rangle$ (●) ordered Mn moments in $ZrMn_6Sn_{5.20}Ga_{0.80}$ below 200 K. The + represent the maximum composite ordered moment in model I. The curves are just guides to the eye.

Table 4. Main parameters for the possible magnetic structures (model I or model II) of $ZrMn_6Sn_{6-x}Ga_x$ ($x = 0.50, 0.60, 0.80$) at 2 K. The fan angle α and the maximum Mn magnetic moment amplitude m_{max} are given for model I. The minimum (m_{min}) and maximum (m_{max}) calculated values of the Mn moments are indicated for model II. See text and figure 8 for details.

		$ZrMn_6Sn_{5.50}Ga_{0.50}$	$ZrMn_6Sn_{5.40}Ga_{0.60}$	$ZrMn_6Sn_{5.20}Ga_{0.80}$
Model I	Type	ANTIFAN-P	ANTIFAN-P	FAN-P
	α (deg)	97	82	140
	m_{max} (μ_B)	2.45	1.66	3.07
Model II	Type	ANTIFAN-E	ANTIFAN-E	DS
	m_{min} (μ_B)	0.31	0.48	0.98
	m_{max} (μ_B)	2.93	2.02	3.10

compositions has still to be determined, it differs from that of $RMn_6Sn_{6-x}X'_x$ with trivalent R as expected from magnetization measurements. During our refinements, we were unable to detect the weak temperature-dependent ferromagnetic component evidenced in the thermomagnetic curve [13] of $ZrMn_6Sn_{5.4}Ga_{0.6}$. We note that, whatever the temperature, the refined Mn moment value for this compound is at least 20% lower than that of other compositions. The reduced refined Mn moment may be explained, at least partially, by assuming that this ferromagnetic component, which may come from a few grains with higher Ga content, does not give rise to coherent scattering due to the lack of long-range order and, consequently, that some of the magnetic intensity is lost.

4.3.4. Magnetic phase diagram. In figure 10, we present a tentative (x, T) phase diagram of $ZrMn_6Sn_{6-x}Ga_x$ which compiles all the data obtained from the present neutron

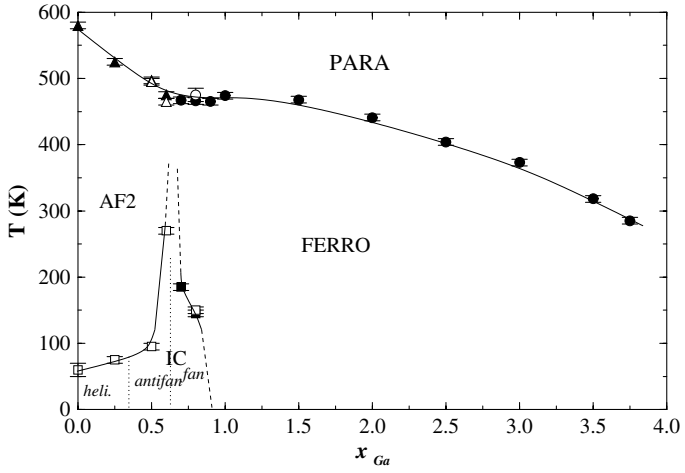

Figure 10. (x, T) magnetic phase diagram of $ZrMn_6Sn_{6-x}Ga_x$ (open symbols: neutron data; full symbols: magnetic measurements). For $0.25 \leqslant x \leqslant 3.75$, the magnetic data are taken from [13]. For $x = 0.0$, both magnetic and neutron data are taken from [3].

diffraction study and from previous magnetic measurements [13]. The precise range of the incommensurate part (IC) as well as those of the underlying magnetic arrangements (helical, *antifan-like* and *fan-like*) are somewhat uncertain and therefore marked with broken lines. The crossover from *antiferromagnetic-like* to *ferromagnetic-like* behaviour takes place within the narrow 0.60–0.70 Ga concentration range in a quite abrupt manner, unlike $RMn_6Sn_{6-x}X'_x$ with trivalent R whose helical q_z component changes smoothly with x [12]. Lifshitz point(s) [20, 26] are expected for $0.60 < x < 0.70$. As explained by Rossat-Mignod [17], the unusual nature of the transition at T_{CI} from a high-temperature commensurate phase to a low-temperature incommensurate (helical) one is a feature of systems close to a Lifshitz point. A Lifshitz point is a special multicritical point where paramagnetic, commensurate and incommensurate phases become indistinguishable [27].

5. Conclusion

Using powder neutron diffraction, the magnetic structures of $HfFe_6Ge_6$-type $ZrMn_6Sn_{6-x}Ga_x$ compounds have been determined. Below their ordering temperature, the compounds adopt either the $+--+$ AF2 arrangement ($x \leqslant 0.60$) or the ferromagnetic structure ($x \geqslant 0.80$). While the ferromagnetic state is stable down to 2 K for $x \geqslant 0.90$, $ZrMn_6Sn_{6-x}Ga_x$ with lower Ga contents present a commensurate–incommensurate transition at a concentration-dependent temperature T_{CI}. The incommensurate magnetic structures below T_{CI} are very likely stabilized due to competitive antiferromagnetic and ferromagnetic RKKY-type interplanar exchange interactions. The gradual evolution of the magnetic order with increasing Ga concentration up to T_{CI} reflects the progressive increase of the ferromagnetic interactions relative to the antiferromagnetic ones. While the compounds with low Ga concentration are helimagnetic, *antifan-like* and *fan-like* structures, observed for the first time within $RMn_6Sn_{6-x}X'_x$ ($X' =$ In or Ga) series, are successively realized upon increasing the Ga content. The precise configuration of the Mn moments in the *(anti)fan-like* structures has still to be determined using, for instance, single-crystal neutron diffractometry. Crystallizations based on molten flux method [12, 28, 29] are currently in progress. Further experiments are also necessary to complete the tentative

(x, T) magnetic phase diagram in the very narrow region ($0.60 < x < 0.70$) where the crossover from antiferromagnetism to ferromagnetism takes place. In this way, the nature of the possible multicritical point(s) could be determined.

Acknowledgments

The Institut Laue Langevin is warmly acknowledged for providing the neutron facilities as well as the CNRS for the use of the CRG D1B instrument.

References

[1] Venturini G, Fruchart D and Malaman B 1996 *J. Alloys Compounds* **236** 102
[2] Mazet T, Venturini G, Welter R and Malaman B 1998 *J. Alloys Compounds* **264** 71
[3] Mazet T, Welter R and Malaman B 1999 *J. Alloys Compounds* **284** 54
[4] Mazet T, Welter R and Malaman B 1999 *J. Magn. Magn. Mater.* **204** 11
[5] Zhang S, Zhao P, Cheng Z, Li R, Sun J, Zhang H and Shen B 2002 *Phys. Rev.* B **64** 212404
[6] Lefevre C, Venturini G, Vernière A and Malaman B 2002 *J. Alloys Compounds* **345** 36
[7] Lefevre C, Venturini G, Vernière A and Malaman B 2002 *J. Alloys Compounds* **334** 53
[8] Canepa F, Napoletano M, Lefevre C and Venturini G 2002 *J. Alloys Compounds* **347** 60
[9] Canepa F, Napoletano M, Lefevre C and Venturini G 2003 *J. Alloys Compounds* **349** 6
[10] Canepa F, Napoletano M, Lefevre C and Venturini G 2003 *Physica* B **334** 68
[11] Lefèvre C, Vernière A, Venturini G and Malaman B 2003 *J. Alloys Compounds* **361** 40
[12] Lefèvre C 2004 *Thèse de l'Université Nancy I* Nancy, France
[13] Mazet T, Emeraux J P and Malaman B 2004 *J. Phys. D: Appl. Phys.* **37** 1305
[14] Mazet T, Tobola J, Venturini G and Malaman B 2002 *Phys. Rev.* B **65** 104406
[15] Rodriguez-Carvajal J 1993 *Physica* B **192** 55
[16] McCusker L B, Von Dreele R B, Cox D E, Loüer D and Scardi P 1999 *J. Appl. Crystallogr.* **32** 36
[17] Rossat-Mignod J 1987 *Methods of Experimental Physics: Neutron Scattering* vol 3 (New York: Academic) p 69
[18] Schobinger-Papamantellos P, Rodriguez-Carvajal J, André G and Buschow K H J 1995 *J. Magn. Magn. Mater.* **150** 311
[19] Schobinger-Papamantellos P, André G, Rodriguez-Carvajal J, Duong N P and Buschow K H J 2001 *J. Magn. Magn. Mater.* **231** 121
[20] Izyumov Yu A 1984 *Sov. Phys.—Usp.* **27** 845
[21] Ishikawa Y, Komatsubara T and Hirahara E 1969 *Phys. Rev. Lett.* **23** 532
[22] Jensen J and Mackintosh A R 1990 *Phys. Rev. Lett.* **64** 2699
[23] Givord D and Lemaire R 1974 *IEEE Trans. Magn.* **10** 109
[24] Lohstroh W, Schulte O, Klose F, Münzenberg M, Felsch W, Maletta H and Lauter H 1997 *Physica* B **234–236** 477
[25] Atoji M 1972 *J. Chem. Phys.* **57** 2402
[26] Selke W 1992 *Phase Transitions and Critical Phenomena* vol 15 (San Diego, CA: Academic) p 1
[27] Hornreich R M, Luban M and Shtrikman S 1975 *Phys. Rev. Lett.* **35** 1678
[28] Canfield P C and Fisk Z 1992 *Phil. Mag.* B **65** 1117
[29] Clatterbuck D M and Gschneidner K A Jr 1999 *J. Magn. Magn. Mater.* **207** 78